Electrochemical interaction of Sn-containing MAX phase (Nb_2SnC) with Li-ions

Shuangshuang Zhao[a], Yohan Dall'Agnese[b], Xuefeng Chu[c], Xin Zhao[a],

Yury Gogotsi[a,d,*], Yu Gao[a,*]

[a]Key Laboratory of Physics and Technology for Advanced Batteries (Ministry of Education), College of Physics, Jilin University, Changchun 130012, PR China

[b]Institute for Materials Discovery, University College London, London WC1E 7JE, United Kingdom

[c]Comprehensive Energy Saving, School of Electrical and Electronic Information Engineering, Jilin Jianzhu University, Changchun 130118, China

[d]A. J. Drexel Nanomaterials Institute, and Department of Materials Science and Engineering, Drexel University, Philadelphia, PA 19104, United States

E-mail：gogotsi@drexel.edu (Y. Gogotsi), yugao@jlu.edu.cn (Y. Gao)

Abstract

In this paper, we report on the interaction of Nb_2SnC ternary transition metal carbide (MAX phase) with Li ions. Because of the presence of Sn layers, which can undergo alloying reaction with Li, this material may be promising for energy storage. Contrary to most electrodes, the performance of this material improves along with the cycle number; specifically, the capacity increases gradually from 87 mAh g^{-1} to 150 mAh g^{-1} at a current density of 500 mA g^{-1} during 600 charge/discharge cycles. Post-cycling study suggests that the alloying reaction makes the material break into smaller particles, increasing capacity. Since Nb_2SnC is just one of many MAX phases, this work lays the foundation for the exploration of the MAX phases in lithium ion or other batteries.

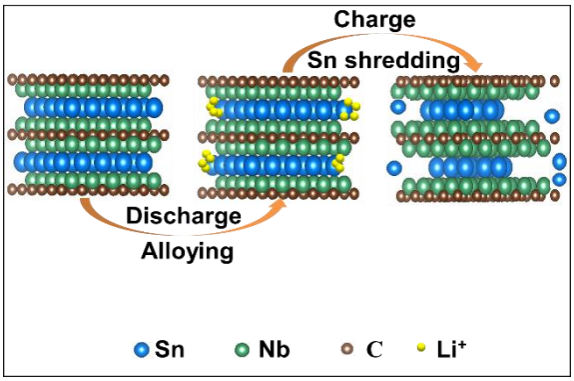

Developing energy conversion and storage device with excellent performance and high stability is remaining an important task [1]. Rechargeable batteries with various ions (Li^+, Na^+, K^+, Mg^{2+}) have become the main means of electrical energy storage. Among those, lithium-ion batteries are the most popular and widely studied because of their high voltage and relatively long cycle-life, but Li-ion capacitors and Li-S batteries also use Li-ions for energy storage. Tin is a prospective negative electrode material because of its attractive theoretical capacity from its alloying reaction with lithium (the theoretical capacity of $Li_{4.4}Sn$ is 994 mAh g^{-1}), which exceeds the capacity of traditional graphite electrodes. However, excessive expansion of tin upon reaction with Li (~ 300 % volume expansion) and poor cyclic stability limit the use of metallic tin as the anode material [2-3]. Usually, carbon additions such as graphene are used to mitigate the volume expansion of Sn and obtained good electrochemical properties, for example, Wang et al. reported that 3D Sn–graphene shows a reversible capacity of 466 mAh g^{-1} at 879 mA g^{-1} with an outstanding cycling stability [4-6].

Since 2011, ternary and 2D transition metal carbides and nitrides labeled MAX phases and their derivatives, MXenes, have attracted increasing attention for applications in the field of energy storage because of their layered structure and metallic conductivity [7-8]. More than 155 kinds of MAX phases have been studied, of general chemical formula $M_{n+1}AX_n$, where M stands for transition metals (such as Ti, Nb, Mo or V), A is the symbol of A-group element (such as Al, Sn or Si), X is carbon and/or nitrogen, and n is an integer from 1 to 3 [9-13].

Herein, we explore Li intercalation behavior of Nb_2SnC, which is one of the few known MAX phases with Sn as the “A” layer. The hypothesis that led to this study was that Nb_2SnC, having the layered structure similar to graphite, offers a metallic conductivity of Nb_2C layers combined with Sn layers in the Nb_2SnC, which have high theoretical capacity. Intercalation of Li into Si and Al containing MAX phases has been investigated in the past, showing promise [7, 14], but no MAX phase with Sn as A-element layers has been studied. This work focuses on exploring the behavior of the MAX phase containing Sn in lithium electrolyte and studying its structural

changes upon cycling, which may provide a basis for the exploration of other MAX phases in the energy storage field.

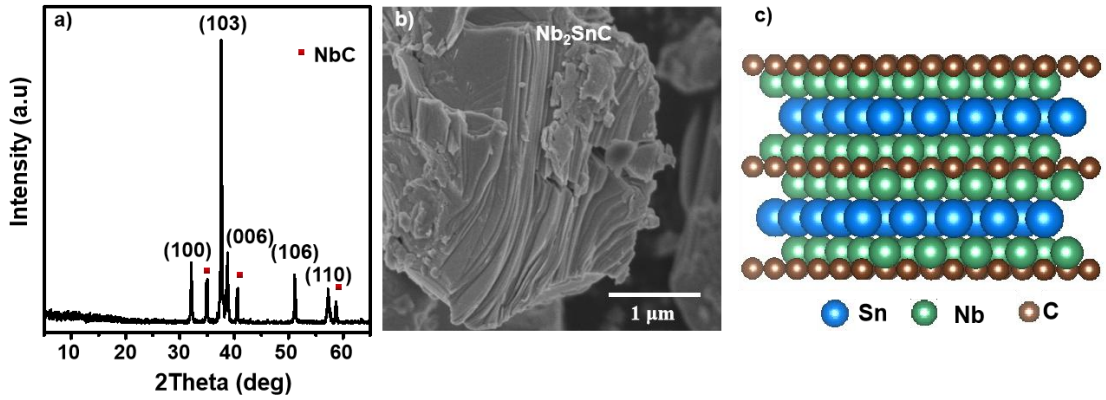

Figure 1. (a) XRD pattern and (b) SEM image of Nb_2SnC. (c) Atomistic structure model of Nb_2SnC.

The XRD pattern and SEM image of Nb_2SnC are shown in Figure 1. The XRD result shows the successful synthesis of Nb_2SnC (PDF # 04-005-0034), although NbC impurity was detected [15]. NbC is a common carbide impurity that is difficult to eliminate during the synthesis of Nb-based MAX phases or by a post-treatment, but NbC does not exhibit any lithium capacity [16-19] and its contribution to the total capacity can be ignored in this study. The bulk Nb_2SnC material seen in Figure 1 (b) displays a typical layered structure with the average particle size of about 2 micrometers (± 0.5 µm). The atomistic structure model of Nb_2SnC is been shown in Figure 1 (c), which is similar to other 211 MAX phases, such as Ti_2AlC and Nb_2AlC. Figure 2 (a) shows a TEM image of Nb_2SnC, which has the typical for a MAX phase morphology. Furthermore, the selected area electron diffraction pattern seen in Figure 2 (b) confirmed the hexagonal single-crystal structure of Nb_2SnC grains [20-21]. Energy dispersive X-ray spectroscopy (EDS) elemental mapping (Figure 2 (c-e)) was used to examine the carbon, niobium, and tin elements distribution in the particle and confirm that all of them are uniformly distributed and the observed particle is Nb_2SnC.

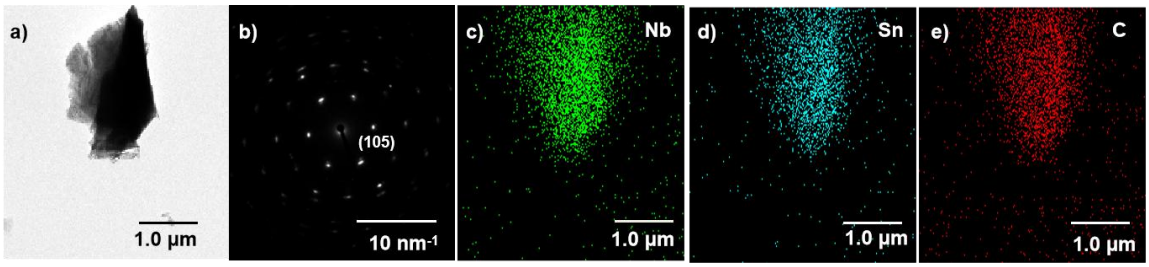

Figure 2. (a) TEM image of Nb_2SnC. (b) SAED pattern. The corresponding elemental mapping of (c) Nb, (d) Sn, and (e) C showing a uniform distribution of the elements within a Nb_2SnC grain.

Figure 3 (a) shows the cyclic voltammetry (CV) curves at a scan rate of 0.1 mV s^{-1} in the voltage window from 0.01-3 V *vs.* Li/Li^+ and compares the CVs of the first two cycles with those of the 501st and 502nd cycles. The existence of two irreversible peaks in the first cycle is attributed to the formation of SEI [22]. It is worth noting that small peaks around 0.5 V and 0.6 V *vs.* Li/Li^+ in the oxidation and reduction profiles, corresponding to alloying reaction of Sn, appeared after cycling. In order to make the peaks more pronounced, a half cell Li-ion battery was assembled using pure Nb_2SnC powder as working electrode (i.e., no conductive additives, no copper foil, no binder). Figure S1 shows the cyclic voltammogram of pure Nb_2SnC powder. The lithiation/delithation reactions: LiSn (0.64 V, 0.81 V), Li_7Sn_3 (0.49 V, 0.74 V), and $Li_{22}Sn_5$ (0.17 V, 0.52 V) confirmed the existence of alloying reaction of Sn [23]. Another broad oxidation peak about 1.2 V and a redox peak at 0.8 V may be the reaction between Li^+ and MAX phase [24]. Comparing the cyclic voltammograms of the 501st and 502nd cycles with the first two cycles, although no redox peak appeared or disappeared, the overall shape of the curve significantly changed as the original redox peaks became broader after 500 cycles. This indicates that the electrochemical capacity was significantly improved. Electrochemical impedance spectroscopy (EIS) at 3 V *vs*. Li/Li^+ (Figure 3 (b)) shows that semicircles' diameter decreased with the cycle number, which may come from the decrease of the charge transfer resistance, indicating a self-improvement of the electrode and rapid electron transport during the electrochemical reactions [25-26], which may be one of the reasons for the increase in capacity. In the Nyquist plots of 501st to 503rd cycles, there is an additional semicircle

corresponding to the SEI film, showing the SEI film's presence on the surface of the material [27-29]. The long cycle performance at the current density of 500 mA g^{-1} and charge/discharge profiles at same current density at different cycles are presented in Figure 3 (c) and (d) respectively. Interestingly, discharge capacity increased along with the cycle number, specifically from about 70 mAh g^{-1} in the first cycle to about 156 mAh g^{-1} after 1500 cycles. The corresponding rate performance of the Nb_2SnC are shown in Figure 4.

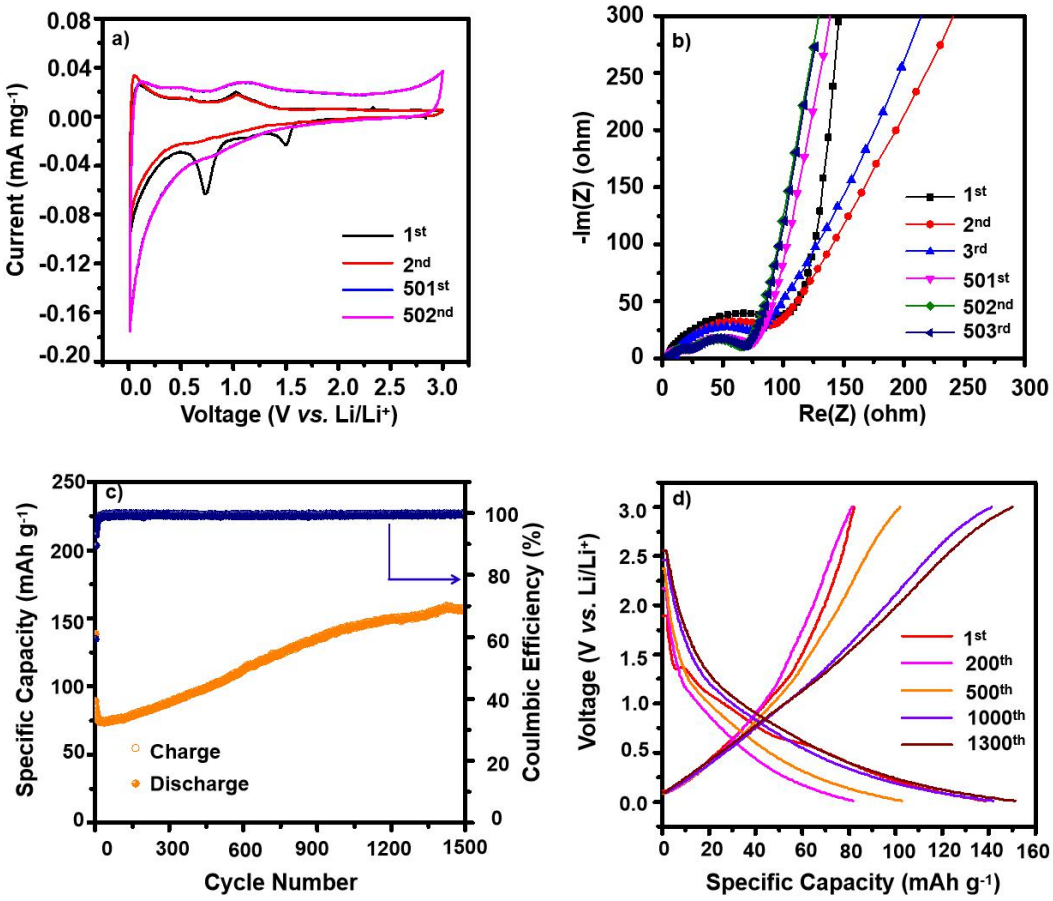

Figure 3. (a) CV curves at a scan rate of 0.1 mV s^{-1}. (b) Nyquist plots from different numbers of cycles. (c) Cycling performance at the current density of 500 mA g^{-1}. (d) Charge-discharge profiles of Nb_2SnC at different cycles with a current density of 500 mA g^{-1}.

The discharge capacities reached 115 mAh g^{-1}, 110 mAh g^{-1}, 102 mAh g^{-1} and 87 mAh g^{-1} at current densities of 50 mA g^{-1}, 100 mA g^{-1}, 200 mA g^{-1} and 500 mA g^{-1}, respectively (Figure 4 (a)). Importantly, the discharge capacity increased from 87

mAh g^{-1} to 150 mAh g^{-1} after 600 cycles at the current density of 500 mA g^{-1} as shown in Figure 4 (b). In contrast to experiment shown Figure 3 (c), results shown Figure 4 (b) were obtained after cycling at lower current densities, which activated the material and accelerated the reaction process. Moreover, after 600 cycles, the rate performance was further improved, as seen Figure 4 (c). At the same current densities of 50 mA g^{-1}, 100 mA g^{-1}, 200 mA g^{-1} and 500 mA g^{-1}, the capacity increased to 234 mAh g^{-1}, 224 mAh g^{-1}, 208 mAh g^{-1} and 151 mAh g^{-1}, respectively, which is almost twice the original values.

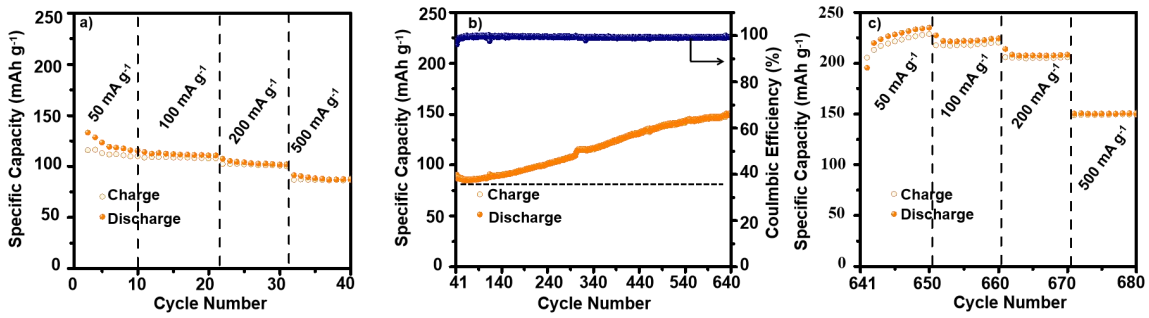

Figure 4. Effect of cycling on electrochemical response of Nb_2SnC. (a) Rate performance of the MAX phase Nb_2SnC. (b) Cycling performance at the current density of 500 mA g^{-1}. (c) Rate performance after long cycling at 500 mA g^{-1}.

Figure S2 shows the XPS spectra for Sn 3d region of Nb_2SnC, before and after cycling. The valence of Sn in the original sample is close to 0 (493.3 eV, 484.8 eV) and traces of Sn^{+4} were observed (495.5 eV, 487.3 eV) [30-34]. Sn^{+4} may come from oxidation of Sn powder during the solid phase sintering process, but its content is negligible. However, after 600 cycles, there is no peak of Sn^0. This means that Sn was largely extracted from the MAX phase, at least from the surface layer analyzed by XPS.

Compared to the morphology of the pristine Nb_2SnC obtain from SEM (Figure 1 (a)), the sample after 600 cycles has gaps between the layers, as shown in Figure 5 (a) and (b). From observing the difference in the cross-sectional SEM images before and after cycling (Figure S3), it can be concluded that the volume of the material increased significantly, even though there may be some SEI film on surface. Moreover, from the TEM images Figure 5 (c), there are many thin and even monolayer

nanosheets. This phenomenon may be caused by the volume expansion of the alloying products during cycling, which makes some layers of the MAX phase appear to be exfoliated. Furthermore, as seen Figure S4, there are some small particles, which could be the Sn (or tin oxide formed after exposure to air) that was extracted from the MAX phase. In the high-resolution transmission electron microscope (HRTEM) images before and after cycling, shown in Figure 5 (d) and (e), the crystal planes of Nb_2SnC are identifiable by the 0.25 nm d-spacing, close to the d-spacing of the (102) planes. After 600 cycles, in addition to Nb_2SnC crystal planes (102), there are two other crystal structures with spacings about 0.33 nm and 0.42 nm. The d-spacing of 0.33 nm is attributed to (110) plane of SnO_2 [35-36], probably coming from the repeated alloying reaction between Sn and Li, resulting in the shredding of a small amount of Sn, which formed SnO_2 when exposed to air. The interlayer spacing of 0.42 nm is probably coming from the etched Nb_2SnC after removal of Sn. In addition, after hundreds of cycles, some smaller, nanometric, Nb_2SnC particles with larger spacing about 0.61 nm appeared, as shown in Figure 5 (f). We suggest that this is due to the lithium ions entering the interlayers, which causes some of the MAX phase to break down into smaller particles. Because of the decrease of particle size and the gradual appearance of interlayer spacing, the specific surface area of Nb_2SnC increases. Therefore, logically the contribution of EDLC/pseudo-capacitance will increase gradually in the subsequent cycles [37]. This conclusion can also be drawn from the CV curves at different scan rates of pristine electrode and after 600 cycles, as shown in Fig. S5. By comparison, the redox peak was obvious initially, but after 600 cycles, the shape of the CV curves is closer to a rectangle and the redox peak is wider, closer to capacitive mechanism, which may be one of the reasons for the capacity increase. Combined with the results of Figure 3-5, we speculate that the Li^+ ion alloyed with the edge of Sn layer in Nb_2SnC, and the larger volume of Li_xSn broke the bond between Sn and Nb_2C layers. Due to the repeated expansion of the outer alloying products, Sn is extracted from the outer layer of MAX phase grains, which leads a somewhat increased layer spacing. However, from the XRD patterns at different voltages and after 600 cycles (Figure S6), there is no obvious peak change occurs in

the discharge process, which could be because only Sn at the edge of the particle was in contact with lithium ions and participated in the alloying reaction, whereas Sn in the bulk was not involved in the redox process. But after 600 cycles, there is little change in XRD result, the peaks widened significantly, which may be due to the smaller particle size.

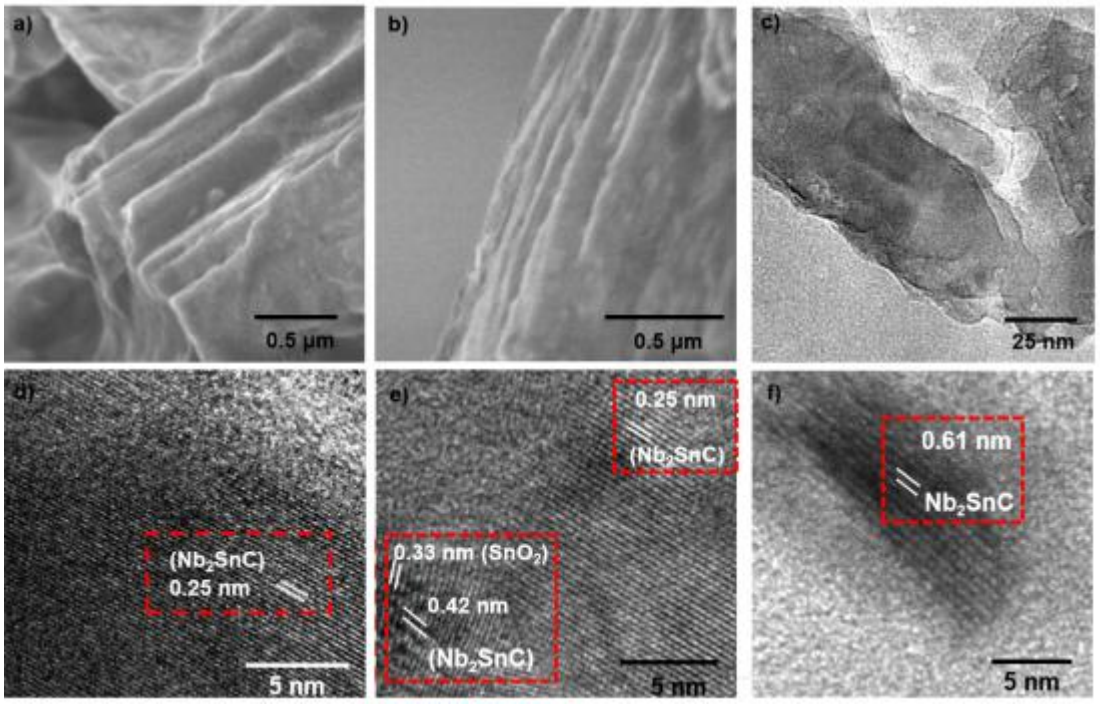

Figure 5. (a-b) SEM images and (c) TEM images of Nb_2SnC electrodes after 600 cycles. HRTEM images (d) before and (e-f) after 600 cycles.

Nb_2SnC is the first reported MAX phase with Sn as the "A" element which shows an attractive electrochemical performance in Li-ion electrolyte. At the current density of 50 mA g^{-1} and 500 mA g^{-1}, the capacity values reached 234 mAh g^{-1} and 151 mAh g^{-1} respectively, and there is a phenomenon of capacity increasing with cycling. The lithium ions react with Sn to form Li_xSn, which can gradually exfoliate a few layers and single layers or Nb_2C, extract Sn from the structure, and break the large MAX phase particles into smaller and more electrochemically active particles, facilitating pseudocapacitive reaction and contributing to capacity improvement [37]. The volume expansion and cracking of the electrode is usually a drawback in most Sn-based electrode, but this work shows that it can be beneficial for highly conductive Nb_2SnC, because it substantially increases its electrochemical performance. MAX

phase Nb_2SnC as anode in batteries combines the advantages of layered materials and alloying elements and has a longer cycle life than most nanomaterials with Sn nanoparticles. These results may provide inspiration for improving the stability of Sn and other alloying materials, as well as exploration of other MAX family members in electrochemical applications.

Supporting Information

The Supporting information is available free of charge.

The synthesis and characterization of Nb_2SnC; Preparation of electrode and electrochemical measurements; CV curves of pure Nb_2SnC powder at a scan rate of 0.1 mV s^{-1}; XPS spectra for Sn 3d region of Nb_2SnC before and after 600 cycles; The cross-sectional SEM images of Nb_2SnC electrodes before and after electrochemical cycling; TEM images of Nb_2SnC electrodes after 600 cycles; CV curves at different scan rate before and after cycling; XRD patterns at different voltages of the second cycle; XRD patterns before and after 600 cycles.

Acknowledgements

This work was financially supported by the Science & Technology Department of Jilin Province (No. 20180101199JC, 20180101204JC), Jilin Province/Jilin University Co-construction Project-Funds for New Materials (SXGJSF2017-3).

References

1. Zuo, X. X.; Zhu, J.; Müller-Buschbaum, P.; Cheng, Y. J. Silicon based lithium-ion battery anodes: A chronicle perspective review. *Nano Energy* **2017**, 31, 113-143.

2. Li, X. F.; Dhanabalan, A.; Gu, L.; Wang, C. L. Three‐Dimensional Porous Core‐Shell Sn@Carbon Composite Anodes for High‐Performance Lithium‐Ion Battery Applications. *Advanced Energy Materials* **2011**, 2, 238-244.

3. Sui, X. Y.; Huang, X. K.; Wu, Y. P.; Ren, R.; Pu, H.H.; Chang, J. B.; Zhou, G. H.; Mao, S.; Chen, J.H. Organometallic Precursor-Derived SnO_2/Sn-Reduced Graphene Oxide Sandwiched Nanocomposite Anode with Superior Lithium Storage Capacity. *ACS Applied Materials & Interfaces* **2018**, 10, 26170-26177.

4. Wang, C. D.; Li, Y.; Chui, Y. G.; Wu, Q. H.; Chen, X. F.; Zhang, W. J. Three-dimensional Sn–graphene anode for high-performance lithium-ion batteries. *Nanoscale* **2013**, 5, 10599-10604.

5. Qin, J.; He, C. N.; Zhao, N. Q.; Wang, Z. Y.; Shi, C. S.; Liu, E. Z.; Li, J. J. Graphene Networks Anchored with Sn@Graphene as Lithium Ion Battery Anode. *ACS Nano* **2014**, 8, 1728-1738.

6. Liu, L. H.; Xie, F.; Liu, J.; Zhao, T. K.; Li, T. H.; Chou, B. G. Tin-based anode materials with well-designed architectures for next-generation lithium-ion batteries. *Journal of Power Sources* **2016**, 321, 11-35.

7. Xu, J. G.; Zhao, M. Q.; Wang, Y. C.; Yao, W.; Chen, C.; Anasori, B.; Sarycheva, A.; Ren, C. E.; Mathis, T.; Gomes, L.; Liang, Z. H.; Gogotsi, Y. Demonstration of Li-Ion Capacity of MAX Phases. *ACS Energy Letters* **2016**, 1, 1094−1099.

8. Anasori, B.; Lukatskaya, M. R.; Gogotsi, Y. 2D metal carbides and nitrides (MXenes) for energy storage. *Nature Reviews Materials* **2017**, 2, 1-17.

9. Zhu, M. S.; Huang, Y.; Deng, Q. H.; Zhou, J.; Pei, Z. X.; Xue, Q.; Huang, Y.; Wang, Z. F.; Li, H. F.; Huang, Q.; Zhi, C. Y. Highly Flexible, Freestanding Supercapacitor Electrode with Enhanced Performance Obtained by Hybridizing Polypyrrole Chains with MXene. *Advanced Energy Materials* **2016**, 6, 1600969.

10. Liang, X.; Rangom, Y.; Kwok, C. Y.; Pang, Q.; Nazar, L. F. Interwoven MXene Nanosheet/Carbon-Nanotube Composites as Li-S Cathode Hosts. *Advanced Materials* **2016**, 29, 1603040.

11. Naguib, M.; Halim, J.; Lu, J.; Cook, K. M.; Hultman, L.; Gogotsi, Y.; Barsoum, M. W. New two-dimensional niobium and vanadium carbides as promising materials for Li-ion batteries. *Journal of the American Chemical Society* **2013**, 135, 15966-15969.

12. Wang, C. D.; Xie, H.; Chen, S. M.; Ge, B. H.; Liu, D. B.; Wu, C. Q.; Xu, W. J.; Chu, W. S.; Babu, G. G.; Ajayan, P. M.; Song, L. Atomic Cobalt Covalently Engineered Interlayers for Superior Lithium-Ion Storage. *Advanced Materials* **2018**, 30, 1802525.

13. Sokol, M.; Natu, V.; Kota, S.; Barsoum, M. W. On the Chemical Diversity of the MAX Phases. *Trends in Chemistry* **2019**, 1, 210-223.

14. Wang, X. F.; Shen, X.; Gao, Y. R.; Wang, Z. X.; Yu, R. C.; Chen, L. Q. Atomic-Scale Recognition of Surface Structure and Intercalation Mechanism of Ti_3C_2X. *Journal of the American Chemical Society* **2015**, 137, 2715-2721.

15. Bortolozo, A. D.; Sant'Anna, O. H.; Luz, M. S. D.; Santos, C. A. M. D.; Pereira, A. S.; Trentin, K. S.; Machado, A. J. S. Superconductivity in the Nb_2SnC compound. *Solid State Communications* **2009**, 139, 57-59

16. Ghidiu, M.; Naguib, M.; Shi, C.; Mashtalir, O.; Pan, L. M.; Zhang, B.; Yang, J.; Gogotsi, Y.; Billinge, S. J.; Barsoum, M. W. Synthesis and characterization of two-dimensional Nb_4C_3 (MXene). *Chemical Communications* **2014**, 50, 9517-9520.

17. Mashtalir, O.; Lukatskaya, M. R.; Zhao, M. Q.; Barsoum, M. W.; Gogotsi, Y. Amine-Assisted Delamination of Nb_2C MXene for Li-Ion Energy Storage Devices. *Advanced Materials* **2015**, 27, 3501-3506.

18. Yang, J.; Naguib, M.; Ghidiu, M.; Pan, L. M.; Gu, J.; Nanda, J.; Halim, J.; Gogotsi, Y.; Barsoum, M. W. Two-Dimensional Nb-Based M_4C_3 Solid Solutions (MXenes). *Journal of the American Ceramic Society* **2016**, 99, 660-666.

19. Hu, J.; Tian, Z. M. Synthesis and electrochemical performance of NbC-modified $LiFePO_4$/C as cathode material for lithium-ion batteries. *Ceramics International* **2015**, 41, 3927-3931.

20. Yu, P.; Cao, G. J.; Yi, S.; Zhang, X.; Li, C.; Sun, X. Z.; Wang, K.; Ma, Y. W. Binder-free 2D titanium carbide (MXene)/carbon nanotube composites for high-performance lithium-ion capacitors. *Nanoscale* **2018**, 10*,* 5906-5913.

21. Naguib, M.; Mochalin, V. N.; Barsoum, M. W.; Gogotsi, Y. 25th Anniversary Article: MXenes: A New Family of Two‐Dimensional Materials. *Advanced Materials* **2014**, 26, 982-982.

22. Luo, J. M.; Tao, X. Y.; Zhang, J.; Xia, Y.; Huang, H.; Zhang, L. Y.; Gan, Y. P.; Liang, C,; Zhang, W. K. Sn^{4+} Ion Decorated Highly Conductive Ti_3C_2 MXene: Promising Lithium-Ion Anodes with Enhanced Volumetric Capacity and Cyclic Performance. *ACS Nano* **2016**, 10, 2491−2499.

23.Chen, Z. X.; Cao, Y. L.; Qian, J. F.; Ai, X. P.; Yang, H. X. Facile synthesis and stable lithium storage performances of Sn-sandwiched nanoparticles as a high capacity anode material for rechargeable Li batteries. *Journal of Materials Chemistry* **2010**, 20, 7266-7271.

24. Luo, J. M.; Zhang, W. K.; Yuan, H. D.; Jin, C. B.; Zhang, L. Y.; Huang, H.; Liang, C.; Xia, Y.; Zhang, J.; Gan, Y. P.; Tao, X. Y. Pillared Structure Design of MXene with Ultralarge Interlayer Spacing for High Performance Lithium-Ion Capacitors. *ACS Nano* **2017**, 11, 2459−2469.

25. Zhang, Y. L.; Mu, Z. J.; Yang, C.; Xu, Z. K.; Zhang, S.; Zhang, X. Y.; Li, Y. J.; Lai, J. P.; Sun, Z. H.; Yang, Y.; Chao, Y. G.; Li, C. G.; Ge, X. X.; Yang, W. X.; Guo, S.

J. Rational Design of MXene/MoS_2-C Nanohybrids for High-Performance Lithium-Sulfur Batteries. *Advanced Functional Materials* **2018**, 28, 1707578.

26. Yao, Y.; Feng, W. L.; Chen, M. L.; Zhong, X. W.; Wu, X. J.; Zhang, H. B.; Yu, Y. Boosting the Electrochemical Performance of Li-S Batteries with a Dual Polysulfides Confinement Strategy. *Small* **2018**, 14, 1802516.

27. Zhao, S. S.; Meng, X.; Zhu, K.; Du, F.; Chen, G.; Wei, Y. J.; Gogotsi, Y.; Gao, Y. Li-ion Uptake and Increase in Interlayer Spacing of Nb_4C_3 MXene. *Energy Storage Materials* **2017**, 8, 42-18.

28. Mahmoud, A.; Chamas, M.; Lippens, P. E. Electrochemical impedance study of the solid electrolyte interphase in $MnSn_2$ based anode for Li-ion batteries. *Electrochimica Acta* **2015**, 184, 387-391.

29. Wu, H.; Chan, G.; Choi, J. W.; Ryu, I.; Yao, Y.; McDowell, M. T.; Lee, S. W.; Jackson, A.; Yang, Y.; Hu, L. B.; Cui, Y. Stable cycling of double-walled silicon nanotube battery anodes through solid-electrolyte interphase control. *Nature Nanotechnology* **2012**, 7, 310-315.

30. Li, J. T.; Swiatowska, J.; Maurice,V.; Seyeux, A.; Huang, L.; Sun, S. G.; Marcus, P. XPS and ToF-SIMS Study of Electrode Processes on Sn−Ni Alloy Anodes for Li-Ion Batteries. *The Journal of physical Chemistry C* **2011**, 115, 7012-7018.

31. Ehinon, K. K. D.; Naille, S.; Dedryvère, R.; Lippens, P. E.; Jumas, J. C.; Gonbeau, D. Ni_3Sn_4 Electrodes for Li-Ion Batteries: Li−Sn Alloying Process and Electrode/Electrolyte Interface Phenomena. *Chemistry of Materials* **2008**, 20, 5388-5398.

32. Hutchison, M. J.; Zhou, P.; Ogle, K.; Scully, J. R. Enhanced Electrochemical Cu Release from Commercial Cu-Sn Alloys: Fate of the Alloying Elements in Artificial Perspiration. *Electrochimica Acta* **2017**, 241, 73-88

33. Yang, S.; Yue, W. B.; Zhu, J.; Ren, Y.; Yang, X. J. Graphene‐Based Mesoporous SnO_2 with Enhanced Electrochemical Performance for Lithium‐Ion Batteries, *Advanced Functional Materials* **2013**, 23, 3570-3576.

34. Xia, L.; Wang, S. Q.; Liu, G. X.; Ding, L. X.; Li, D. D.; Wang, H. H.; Qiao, S. Z. Flexible SnO_2/N‐Doped Carbon Nanofiber Films as Integrated Electrodes for Lithium‐Ion Batteries with Superior Rate Capacity and Long Cycle Life. *Small* **2016**, 12, 853-859.

35. Liu, J.; Kopold, P.; Wu, C.; van Aken, P. A.; Maier, J.; Yu, Y. Uniform yolk–shell Sn_4P_3@C nanospheres as high-capacity and cycle-stable anode materials for sodium-ion batteries. *Energy & Environmental Science* **2015**, 8, 3531-3538.

36. Al-Enizi, A. M.; Naushad, M.; Al-Muhtaseb, A.; Ruksana.; Alshehri, S. M.;

Alothman, Z. A.; Ahamad, T. Synthesis and characterization of highly selective and sensitive Sn/SnO_2/N-doped carbon nanocomposite (Sn/SnO_2@NGC) for sensing toxic NH_3 gas. *Chemical Engineering Journal* **2018**, 345, 58-66.

37. Simon, P.; Gogotsi, Y.; Dunn, B. Where Do Batteries End and Supercapacitors Begin? *Science* **2014**, 343, 6176.